EURASIP Journal on Advances in Signal Processing
a SpringerOpen Journal

RESEARCH Open Access

An imaging algorithm based on keystone transform for one-stationary bistatic SAR of spotlight mode

Xiaolan Qiu[1,2*], Florian Behner[3], Simon Reuter[3], Holger Nies[3], Otmar Loffeld[3], Lijia Huang[1,2], Donghui Hu[1,2] and Chibiao Ding[1]

Abstract

This article proposes an imaging algorithm based on Keystone Transform for bistatic SAR with a stationary receiver. It can efficiently be applied to high-resolution spotlight mode, and can directly be process the bistatic SAR data which have been ranged compressed by the synchronization reference pulses. Both simulation and experimental results validate the good performance of this algorithm.

Keywords: Bistatic SAR, Imaging algorithm, Keystone transform

Introduction

Bistatic SAR is more flexible in data acquisition geometry compared with traditional monostatic SAR. However, this flexibility is gained at the cost of increasing system complexity, which not only refers to increasing hardware system complexity due to synchronization needs of transmitter and receiver, but also refers to increasing processing complexity. As for the synchronization, the easy to realize and commonly used strategy is using an additional antenna to receive the direct pulses from transmitter, and then using these directly received pulses as a reference for range compression. As for bistatic SAR imaging, a number of studies have been done and several kinds of imaging algorithms have been proposed for different configurations [1-9]. Furthermore, a number of bistatic SAR experiments with different configurations [10-15] have successfully been carried out till now.

Among the various configurations of bistatic SAR, the so-called one-stationary configuration, which is usually formed by an existing moving transmitter (i.e., spaceborne SAR, airborne SAR, or even navigation satellite [16]) and a stationary passive receiver, is, in the authors' opinion, one of the most practical configurations. On the one hand, it is inexpensive to build, and on the other hand, it can easily be extended to multi-receiver stations and then obtain multi-baseline interferometric SAR images to rebuild accurate DEM of regions of interest.

The main difficulty of imaging processing for the one-stationary bistatic configuration has been pointed out and solved to some extent in the authors' previous publication [17,18]. However, the former algorithm mainly aims at the stripmap mode and may not be suitable for the high-resolution spotlight mode. In spotlight mode, the pulse repetition frequency (PRF) is usually smaller than the Doppler bandwidth of a single target. So, the dechirp method is commonly used for efficient processing. Meanwhile, if range compression is done by the directly received pulses from the synchronization channel, the dechirp in azimuth has already been done within this range compressing step. After this dechirp step, the residual range and phase histories are still range–azimuth variant, while the linear term is predominant. In the high-resolution case, the range histories are bending more severely as the range bins are smaller. Hence, the differential range histories for those targets with the same bistatic range will exceed one range gate; therefore, the precondition of the NLCS algorithm based on azimuth perturbation in [18] is no longer valid. Till now, almost all the published images of the one-stationary bistatic SAR experiments have been focused by the universal back-projection (BP) algorithm [10,16]. Although

* Correspondence: xlqiu@mail.ie.ac.cn
[1]Institute of Electronics, Chinese Academy of Sciences, Beijing 100190, China
[2]Key Laboratory of Spatial Information Processing and Applied System, Chinese Academy of Sciences, Beijing 100190, China
Full list of author information is available at the end of the article

good quality images can be obtained using this algorithm, the main shortcoming is its computational inefficiency. The computation load of BP algorithm for producing an image, whose size is $M * M$ and the synthetic aperture length is K, is on the order of M^*M^*K (i.e., $O(M^*M^*K)$). This can be very large for a big size high-resolution image.

In this article, an efficient imaging algorithm based on the Keystone Transform for one-stationary bistatic SAR, whose computation load is on the order of $M^2\log_2 M$, is proposed. The Keystone Transform is usually used in ISAR processing. The idea of using this transform to correct the azimuth variant range cell migration (RCM) in medium-earth–orbit SAR imaging has been proposed in the authors' another article (H Lijia, Q Xiaolan, H Donghui, D Chibiao, A novel algorithm based on keystone transform and azimuth perturbation for medium-earth-orbit SAR, submitted). In this study, we propose to use the Keystone Transform for bistatic SAR imaging. The approach can directly be performed on bistatic SAR data which has been range compressed by the synchronization reference pulses, which makes it convenient to use. The experimental data of the HITCHHIKER system at University of Siegen/ZESS is used to test this algorithm, and good bistatic SAR images are obtained by this algorithm.

This article is organized as follows: "Geometry and signal model" section describes the one-stationary bistatic SAR geometry, and builds the signal model; "Imaging algorithm based on Keystone Transform" section introduces the proposed imaging algorithm step-by-step and shows the block diagram of the algorithm; " Simulation and experimental results" section validates the imaging algorithm through simulations and experimental results, and "Conclusion" section concludes the article.

Geometry and signal model

One-stationary bistatic SAR geometry

The one-stationary bistatic SAR geometry is illustrated in Figure 1. In some Earth-fixed coordinates, the vector of stationary receiver location is $\mathbf{R_R} = (X_R, Y_R, Z_R)^T$. The vector of the moving transmitter is $\mathbf{R_T}(\eta) = [X_T(\eta), Y_T(\eta), Z_T(\eta)]^T$, when the azimuth time (slow time) is η. An arbitrary point scatter on the earth is denoted as $\mathbf{r} = (x, y, z)^T$.

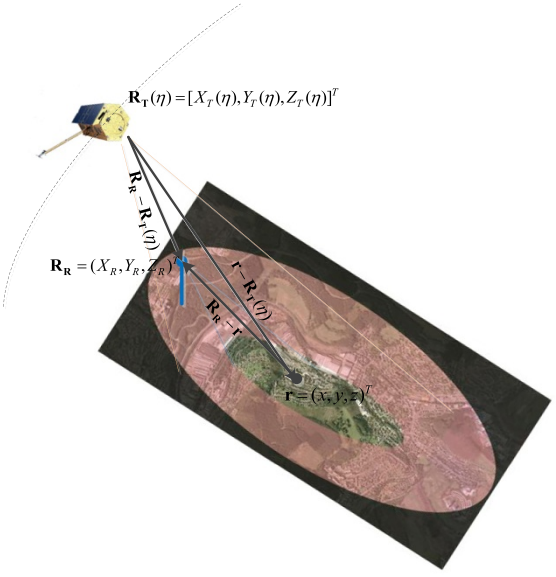

Figure 1 Bistatic SAR geometry of one-stationary configuration.

Signal model

If the time when the received echo reaches the maximum power is considered as $\eta = 0$, the range history of the direct pulses and that of the target $\mathbf{r}$ in spotlight mode can be, respectively, represented as follows.

$$R_D(\eta) = |\mathbf{R_R} - \mathbf{R_T}(\eta)| \tag{1}$$

$$R_{bi}(\eta; \mathbf{r}) = |\mathbf{r} - \mathbf{R_T}(\eta)| + |\mathbf{r} - \mathbf{R_R}| \tag{2}$$

If the nominal frequency of the transmitted signal is f_{0T} and the transmitted signal has a rectangular envelope with a time duration T and a wide bandwidth, the received signal in direct channel and echo channel before down conversion at time $\eta + \tau$ can be written as follows, respectively,

$$\begin{aligned} g_D(\eta, \tau) \approx & w_D(\eta, \tau)\,\mathrm{rect}\left[\frac{\tau - R_D(\eta)/c}{T}\right] p[\tau - R_D(\eta)/c] \\ & \cdot \exp\{j2\pi f_{0T}[\eta + \tau - R_D(\eta)/c] \\ & + j\phi_T[\eta + \tau - R_D(\eta)/c]\} \end{aligned} \tag{3}$$

$$g(\eta, \tau) \approx \iint_{x,y} \left\{ \begin{array}{l} w(\eta, \tau; \mathbf{r})\sigma(\mathbf{r})\,\mathrm{rect}\left[\dfrac{\tau - R_{bi}(\eta; \mathbf{r})/c}{T}\right] \\ \cdot p[\tau - R_{bi}(\eta; \mathbf{r})/c] \\ \cdot \exp\{j2\pi f_{0T}[\eta + \tau - R_{bi}(\eta; \mathbf{r})/c]\} \\ \cdot \exp\{j\phi_T[\eta + \tau - R_{bi}(\eta; \mathbf{r})/c]\} \end{array} \right\} dxdy \tag{4}$$

where $p(\tau)$ represents the transmitted waveform; τ represents the fast time (range time), whose origin is when the pulse is transmitted; ϕ_T is the phase error of the transmitter oscillator; $\sigma(\mathbf{r})$ is the scattering coefficient of target $\mathbf{r}$; $w_D(\eta, \tau)$ and $w(\eta, \tau; \mathbf{r})$ mean the weight due to the transmitter and receiver antenna pattern, propagation loss, etc. Without loss of generality, $w(\eta, \tau; \mathbf{r})$ and $w_D(\eta, \tau)$ are considered as constants here and are ignored in the following analysis.

The approximate equal marks in Equations (3) and (4) come from neglecting the variation of R_D and R_{bi} with τ, respectively.

If the nominal frequency of the receiver is f_{0R}, the down conversion signal at $\eta + \tau$ is then

$$g_R(\eta+\tau) = \exp\{-j2\pi f_{0R}(\eta+\tau) - j\phi_R(\eta+\tau)\} \quad (5)$$

where ϕ_R is the phase error of the receiver oscillator.

Hence, after down conversion, the direct channel signal is

$$\begin{aligned} s_D(\eta,\tau) = {} & \mathrm{rect}\left[\frac{\tau - R_D(\eta)/c}{T}\right] p[\tau - R_D(\eta)/c] \\ & \cdot \exp\{-j2\pi f_{0T} R_D(\eta)/c\} \\ & \cdot \exp\{j2\pi(f_{0T} - f_{0R})(\eta+\tau)\} \\ & \cdot \exp\{j\phi_T[\eta+\tau - R_D(\eta)/c] - j\phi_R(\eta+\tau)\} \end{aligned} \quad (6)$$

and the echo channel signal is

$$s(\eta,\tau) = \iint_{x,y} \left\{ \begin{array}{l} \sigma(\mathbf{r})\,\mathrm{rect}\left[\dfrac{\tau - R_{bi}(\eta;\mathbf{r})/c}{T}\right] p \\ \left[\tau - \dfrac{R_{bi}(\eta;\mathbf{r})}{c}\right] \\ \cdot \exp\{-j2\pi f_{0T} R_{bi}(\eta;\mathbf{r})/c\} \\ \cdot \exp\{j2\pi(f_{0T} - f_{0R})(\eta+\tau)\} \\ \cdot \exp\{j\phi_T[\eta+\tau - R_{bi}(\eta)/c] \\ \quad -j\phi_R(\eta+\tau)\} \end{array} \right\} dxdy \quad (7)$$

Compress $s(\eta,\tau)$ in range direction using $s_D(\eta,\tau)$, which is

$$\begin{aligned} s_1(\eta,\tau) = \mathrm{IFFT}^{\tau}\big[& \mathrm{shift}\{\mathrm{FFT}^{\tau}[s(\eta,\tau)] \\ & \cdot \mathrm{conj}\{\mathrm{FFT}^{\tau}[s_D(\eta,\tau)]\}\}\big] \end{aligned} \quad (8)$$

Here, *shift* means to shift the spectrum which is centered at $f_{0T} - f_{0R}$ to be centered at zero in the range frequency domain and *conj* means conjugation. Then we have

$$s_1(\eta,\tau) \approx \iint_{x,y} \left\{ \begin{array}{l} \sigma(\mathbf{r})\,\mathrm{sinc}\left[\tau - \dfrac{R_{bi}(\eta;\mathbf{r}) - R_D(\eta)}{c}\right] \\ \cdot \exp\{-j2\pi f_{0T}[R_{bi}(\eta;\mathbf{r}) - R_D(\eta)]/c\} \end{array} \right\} dxdy \quad (9)$$

The approximation in the above equation comes from omitting of the phase difference between $\mathrm{rect}\left[\frac{\tau - R_D(\eta)/c}{T}\right] \exp\{-j\phi_R(\eta+\tau)\}$ and $\mathrm{rect}\left[\frac{\tau - R_{bi}(\eta;\mathbf{r})/c}{T}\right] \exp\{-j\phi_R(\eta+\tau)\}$, which can usually be ignored.

It can be seen from Equation (9) that, after range compression using the reference signal from the direct channel, the time synchronization problem is solved because all the received echo pulses are aligned to the known $R_D(\eta)$. The frequency synchronization problem is solved because the direct and the echo pulses are generated by the same transmitter. The phase synchronization is also solved as long as no additional phase difference is introduced by the two receive channels. This is because the phase errors caused by the transmitter are the same in direct and echo pulses and hence can be counteracted; besides, as the direct and the echo pulses are received with small time difference, the phase errors caused by the receiver in direct and in echo pulses are nearly the same and also can be counteracted. So, as has been said in the introduction, this is the easiest and commonly used synchronization method. Therefore, it is reasonable to start bistatic SAR focusing from $s_1(\eta,\tau)$.

The residual range history after range compression is

$$R_{bic}(\eta;\mathbf{r}) = R_{bi}(\eta;\mathbf{r}) - R_D(\eta) \quad (10)$$

It can be seen that, if the receiver is near the scenario, the higher order terms in $R_{bic}(\eta;\mathbf{r})$ will be much smaller than those in the original range history $R_{bi}(\eta;\mathbf{r})$, so the Doppler bandwidth of the targets after range compression by the reference pulses is much smaller than the original Doppler bandwidth. For example, in the spaceborne-ground bistatic SAR configuration, such as in TerraSAR-X/HITCHHIKER experiment, the original Doppler bandwidth is about 5192 Hz, but after the range compression using the direct pulses, the residual Doppler bandwidth shrinks to be about 62 Hz. Therefore, if traditional imaging algorithms, which correct RCM in the azimuth frequency domain, are applied, a Doppler wideband signal rebuilding step should be adopted, which makes them not very convenient to use. In the next section, an algorithm based on the Keystone Transform which does not need Doppler signal rebuilding will be introduced.

Imaging algorithm based on Keystone Transform

Keystone Transform for linear RCM correction

In one-stationary spotlight bistatic SAR cases, such as spaceborne-ground cases and straight path airborne-ground cases, the residual range history can be approximated as follows:

$$R_{bic}(\eta;\mathbf{r}) \approx R_{bic}(0;\mathbf{r}) + A\eta + B\eta^2 + C\eta^3 + D\eta^4 \quad (11)$$

where A,B,C,D are functions of the target position $\mathbf{r}$. In case of simple trajectories such as uniform linear motion, the formula of these parameters A,B,C,D can be obtained as derivatives of $R_{bic}(\eta;\mathbf{r})$. For example, if the

transmitter flies along y-axis with a constant velocity V_T, then the parameters A and B are as follows

$$A(\mathbf{r}) = V_T\left[\frac{Y_T(0)-y}{|\mathbf{r}-\mathbf{R_T}(0)|}-\frac{Y_T(0)-Y_R}{|\mathbf{R_R}-\mathbf{R_T}(0)|}\right] \tag{12}$$

$$B(\mathbf{r}) = {V_T}^2\left[\frac{cos^2\theta_T(\mathbf{r})}{|\mathbf{r}-\mathbf{R_T}(0)|}-\frac{cos^2\theta_T(\mathbf{R_R})}{|\mathbf{R_R}-\mathbf{R_T}(0)|}\right] \tag{13}$$

where

$$\theta_T(\mathbf{r}) = \cos^{-1}\left\{\frac{\sqrt{[X_T(0)-x]^2+[Z_T(0)-z]^2}}{|\mathbf{r}-\mathbf{R_T}(0)|}\right\} \tag{14}$$

$$\theta_T(\mathbf{R_R}) = \cos^{-1}\left\{\frac{\sqrt{[X_T(0)-X_R]^2+[Z_T(0)-Z_R]^2}}{|\mathbf{R_R}-\mathbf{R_T}(0)|}\right\} \tag{15}$$

It can be seen that $A(\mathbf{r})$ nearly linearly depends on y, which means it is strongly azimuth variant, while $B(\mathbf{r})$ depends on $|\mathbf{r}-\mathbf{R_T}(0)|$ and $\theta_T(\mathbf{r})$, which is more slightly azimuth variant than $A(\mathbf{r})$. The higher-order terms are much smaller than the first two-order terms, so here we pay more attention to $A(\mathbf{r})$ and $B(\mathbf{r})$.

In case of a complex trajectory, these parameters can numerically be obtained by polynomial fit to the residual range history.

After performing a range Fourier transform on $s_1(\eta,\tau)$, we have

$$\begin{aligned} S_1(\eta,f) &= \iint_{x,y}\sigma(\mathbf{r})\exp\left\{-j2\pi\frac{f_{0T}+f}{c}R_{\boldsymbol{bic}}(\eta;\mathbf{r})\right\}dxdy \\ &\approx \iint_{x,y}\left\{\begin{array}{l}\sigma(\mathbf{r})\exp\left\{-j2\pi\frac{f_{0T}+f}{c}R_{\boldsymbol{bic}}(0;\mathbf{r})\right\}\\ \cdot\exp\left\{-j2\pi\frac{f_{0T}+f}{c}\left(A\eta+B\eta^2+C\eta^3+D\eta^4\right)\right\}\end{array}\right\}dxdy \end{aligned} \tag{16}$$

The Keystone Transform for linear decoupling is as follows. Let

$$\xi = \frac{f_{0T}+f}{f_{0T}}\eta \tag{17}$$

then

$$S_1(\xi,f)\approx\iint_{x,y}\left\{\begin{array}{l}\sigma(\mathbf{r})\cdot\exp\left\{-j2\pi\frac{f_{0T}+f}{c}R_{bic}(0;\mathbf{r})\right\}\\ \cdot\exp\left\{-j\frac{2\pi}{\lambda}A\xi\right\}\exp\left\{-j\frac{2\pi}{\lambda}\left(\frac{f_{0T}}{f_{0T}+f}\right)B\xi^2\right\}\\ \cdot\exp\left\{-j\frac{2\pi}{\lambda}\left(\frac{f_{0T}}{f_{0T}+f}\right)^2C\xi^3\right\}\\ \cdot\exp\left\{-j\frac{2\pi}{\lambda}\left(\frac{f_{0T}}{f_{0T}+f}\right)^3D\xi^4\right\}\end{array}\right\}dxdy \tag{18}$$

where $\lambda = c/f_{0T}$.

In the general SAR case, $|f| << f_{0T}$, so the following approximation can be applied.

$$\frac{f_{0T}}{f_{0T}+f}\approx 1-\frac{f}{f_{0T}}+\left(\frac{f}{f_{0T}}\right)^2-\left(\frac{f}{f_{0T}}\right)^3 \tag{19}$$

$$\left(\frac{f_{0T}}{f_{0T}+f}\right)^2\approx 1-2\frac{f}{f_{0T}}+3\left(\frac{f}{f_{0T}}\right)^2-4\left(\frac{f}{f_{0T}}\right)^3 \tag{20}$$

$$\left(\frac{f_{0T}}{f_{0T}+f}\right)^3\approx 1-3\frac{f}{f_{0T}}+6\left(\frac{f}{f_{0T}}\right)^2-10\left(\frac{f}{f_{0T}}\right)^3 \tag{21}$$

Substituting Equations (19)–(21) into Equation (18) and reorganizing yields

$$S_1(\xi,f)\approx\iint_{x,y}\left\{\begin{array}{l}\sigma(\mathbf{r})\exp\left\{-j\frac{2\pi}{\lambda}\frac{f_{0T}+f}{f_{0T}}R_{bic}(0;\mathbf{r})\right\}\\ \cdot\exp\{-j\psi_A(\xi;\mathbf{r})\}\\ \cdot\exp\left\{-j\psi_{coup}(\xi,f;\mathbf{r})\right\}\end{array}\right\}dxdy \tag{22}$$

where

$$\psi_A(\xi;\mathbf{r}) = \frac{2\pi}{\lambda}\left(A\xi+B\xi^2+C\xi^3+D\xi^4\right) \tag{23}$$

is the azimuth phase which only depends on ξ. And

$$\begin{aligned}\psi_{\mathrm{coup}}(\xi,f;\mathbf{r}) = &\frac{2\pi}{\lambda}\frac{f}{f_{0T}}\left(-B\xi^2-2C\xi^3-3D\xi^4\right)\\ &+\frac{2\pi}{\lambda}\left(\frac{f}{f_{0T}}\right)^2\left(B\xi^2+3C\xi^3+6D\xi^4\right)\\ &+\frac{2\pi}{\lambda}\left(\frac{f}{f_{0T}}\right)^3\left(-B\xi^2-4C\xi^3-10D\xi^4\right)\end{aligned} \tag{24}$$

is the phase containing the azimuth–range coupling. It can be seen from this phase that no linear coupling between f and ξ exists, which means that the linear RCMs for all targets have been corrected by the Keystone Transform. Then, a bulk phase compensation according to the reference target can be done by the following function

$$\begin{aligned}H_{\boldsymbol{comp}}(\xi,f) = &\exp\left\{-j\frac{2\pi}{\lambda}\left(\frac{f}{f_{0T}}\right)\left(B_{\boldsymbol{ref}}\xi^2+2C_{ref}\xi^3+3D_{\boldsymbol{ref}}\xi^4\right)\right\}\\ &\cdot\exp\left\{j\frac{2\pi}{\lambda}\left(\frac{f}{f_{0T}}\right)^2\left(B_{\boldsymbol{ref}}\xi^2+3C_{ref}\xi^3+6D_{\boldsymbol{ref}}\xi^4\right)\right\}\\ &\cdot\exp\left\{-j\frac{2\pi}{\lambda}\left(\frac{f}{f_{0T}}\right)^3\left(B_{\boldsymbol{ref}}\xi^2+4C_{ref}\xi^3+10D_{\boldsymbol{ref}}\xi^4\right)\right\}\end{aligned} \tag{25}$$

where subscript *ref* means the value calculated at the reference position (usually to be the scene center). Here, we denote $S_2(\xi,f) = S_1(\xi,f)H_{\mathrm{comp}}(\xi,f)$.

Because B,C,D are all changing with $\mathbf{r}$, there is a coupled phase remaining in $S_2(\xi,f)$. The second- and

higher-order terms of f/f_{0T} in the remaining coupled phase will decrease the range focusing quality. Usually, if the quadratic phase error is smaller than π/4, the imaging quality is acceptable. So, the following condition is used to restrict the processing area.

$$\max\left\{\frac{2\pi}{\lambda}\left(\frac{f_B}{2f_{0T}}\right)^2\left|[B(\mathbf{r})-B_{\mathbf{ref}}]\xi^2+3[C(\mathbf{r})-C_{\mathbf{ref}}]\xi^2+6[D(\mathbf{r})-D_{\mathbf{ref}}]\xi^2\right|\right\}\le\frac{\pi}{4} \tag{26}$$

This ensures that in each processing area, all targets $\mathbf{r}$ at each ξ have quadratic phase error that smaller than π/4, so the imaging quality is guaranteed.

Residual RCM correction

If the higher-order term phases of $S_2(\xi,f)$ are restricted and their effects can be neglected. Then, applying an inverse Fourier transform to $S_2(\xi,f)$, the signal in the time domain is

$$s_2(\xi,\tau)\approx\iint_{x,y}\left\{\begin{array}{l}\sigma(\mathbf{r})\exp\left\{-j\frac{2\pi}{\lambda}R_{\mathrm{bic}}(0;\mathbf{r})\right\}\\ \cdot\operatorname{sinc}\left(\tau-\frac{R_{\mathrm{bic}}(0;\mathbf{r})-R^r_{\mathrm{RCM}}(\xi;\mathbf{r})}{c}\right)\\ \cdot\exp\{-j\psi_A(\xi;\mathbf{r})\}\end{array}\right\}dxdy \tag{27}$$

where

$$R^r_{\mathrm{RCM}}(\xi;\mathbf{r})=(B-B_{\mathrm{ref}})\xi^2+2(C-C_{\mathrm{ref}})\xi^3+3(D-D_{\mathrm{ref}})\xi^4 \tag{28}$$

It can be seen that the position of a target in the image plane along the fast time axis is determined by $R_{\mathrm{bic}}(0;\mathbf{r})$, and the residual RCM is a function of the target location, which is range–azimuth variant. Usually, the RCM, which is within half a slant range resolution cell ρ_r, can

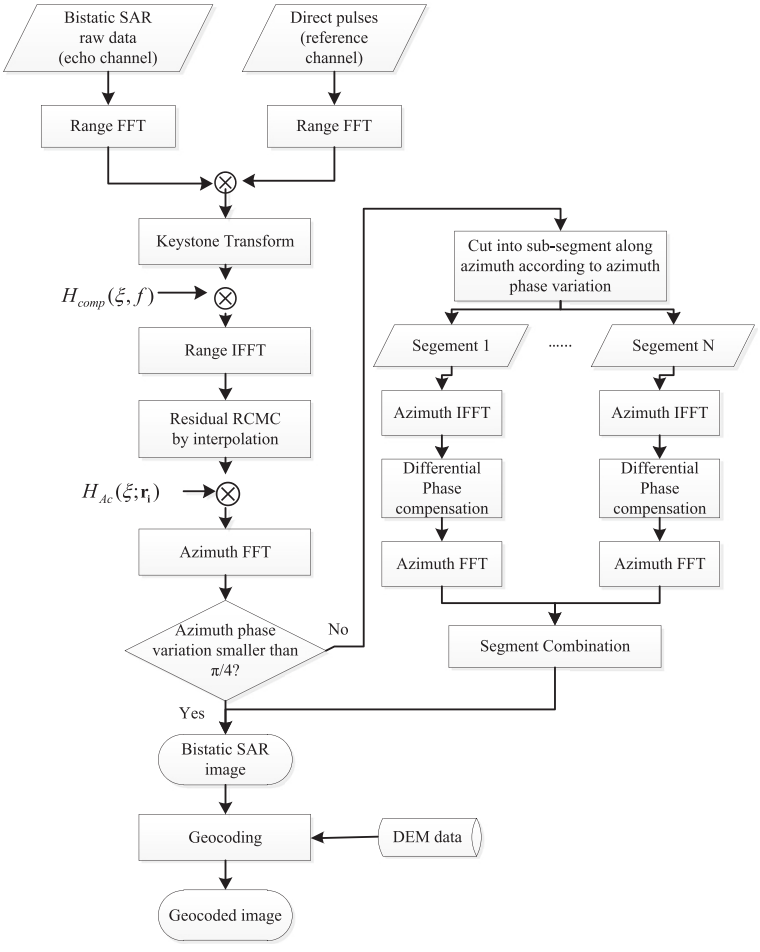

Figure 2 Block diagram of the proposed algorithm for one-stationary bistatic SAR of spotlight mode.

Table 1 Transmitter and receiver parameters for simulation

Symbol	Meaning	Quantity
f_{0T}	Transmitter frequency	9.65 GHz
f_B	Signal bandwidth	300 MHz
f_s	Sample rate	330 MHz
PRF	PRF	3224.35 Hz
f_{0R}	Receiver frequency	9.70 GHz
T_a	Data acquisition time	2.48 s
N_a	Azimuth pulse number	8000
N_r	Range sample number	30000

be neglected in SAR imaging field. So, if the following restriction

$$\max\left\{\left|R^r_{\mathrm{RCM}}(\xi;\mathbf{r})\right|\right\} < \frac{\rho_r}{2} \tag{29}$$

is satisfied for any $\mathbf{r}$, then residual RCM correction step can be omitted. If this cannot be satisfied for the whole scene, then the sub-swath strategy can be used to deal with the azimuth variance and interpolation in two-dimensional time domain can correct the range variance of $R^r_{\mathrm{RCM}}(\xi;\mathbf{r_i})$.

The sub-swath dealing with the azimuth variance is as follows. First, a reference position $\mathbf{r_i}$ is chosen for each range gate i (usually choose to be in the middle of azimuth swath). Then, the azimuth processing sub-swath is restricted according to the following condition

$$\max\left\{\left|R^r_{\mathrm{RCM}}(\xi;\mathbf{r}) - R^r_{\mathrm{RCM}}(\xi;\mathbf{r_i})\right|\right\} < \rho_r/2 \tag{30}$$

Consider the main component (i.e., the second-order term) in $|R^r_{\mathrm{RCM}}(\xi;\mathbf{r}) - R^r_{\mathrm{RCM}}(\xi;\mathbf{r_i})|$ and calculate the above restriction, we have

$$\begin{aligned}
&\max\left\{\left|R^r_{\mathrm{RCM}}(\xi;\mathbf{r}) - R^r_{\mathrm{RCM}}(\xi;\mathbf{r_i})\right|\right\} \\
&\approx \max\left\{V_T{}^2\xi^2\left|\frac{\cos^2\theta_T(\mathbf{r})}{|\mathbf{r}-\mathbf{R_T}(0)|} - \frac{\cos^2\theta_T(\mathbf{r_i})}{|\mathbf{r_i}-\mathbf{R_T}(0)|}\right|\right\} \\
&\approx \max\left\{\frac{V_T{}^2\xi^2}{|\mathbf{r_i}-\mathbf{R_T}(0)|}\left|\cos^2\theta_T(\mathbf{r}) - \cos^2\theta_T(\mathbf{r_i})\right|\right\} < \frac{\rho_r}{2}
\end{aligned} \tag{31}$$

It can be seen that the azimuth sub-swath can be restricted through $\theta_T(\mathbf{r})$, and the limitation of $\theta_T(\mathbf{r})$ is variant with range.

Azimuth compression

After the above steps, the final azimuth compression step can be done. The higher-order term of $\psi_A(\xi;\mathbf{r})$, which is

$$\psi^h_A(\xi;r) = \frac{2\pi}{\lambda}\left(B\xi^2 + C\xi^3 + D\xi^4\right) \tag{32}$$

is desired to be removed for fine focusing. If the azimuth variation of $\psi^h_A(\xi;\mathbf{r})$ is smaller than π/4, then for each range gate, the following phase compensation filter is applied

$$H_{\mathrm{Ac}}(\xi;\mathbf{r_i}) = \exp\left\{j\frac{2\pi}{\lambda}\left[B(\mathbf{r_i})\xi^2 + C(\mathbf{r_i})\xi^3 + D(\mathbf{r_i})\xi^4\right]\right\} \tag{33}$$

Then the final focused image can be obtained through azimuth Fourier transform. The final image can be written as

$$s_3(f_\xi,\tau) = \iint_{x,y}\left\{\begin{array}{l}\sigma(\mathbf{r})\exp\left\{-j\frac{2\pi}{\lambda}R_{\mathrm{bic}}(0;\mathbf{r})\right\} \\ \cdot\,\mathrm{sinc}\left(\tau - \frac{R_{bic}(0;\mathbf{r})}{c}\right)\cdot\mathrm{sinc}\left(f_\xi + \frac{A(\mathbf{r})}{\lambda}\right)\end{array}\right\}dxdy \tag{34}$$

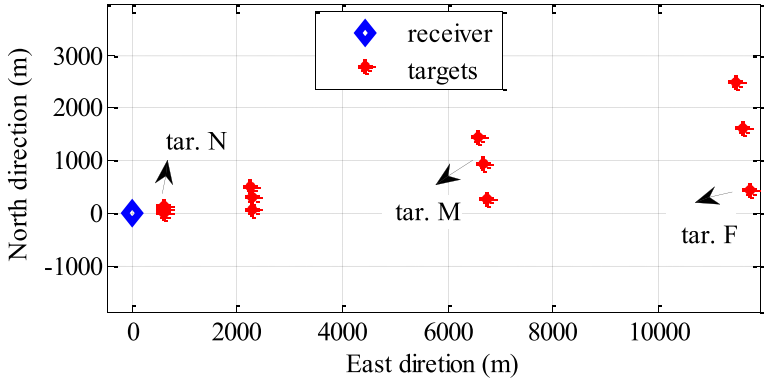

Figure 3 Locations of the targets and the receiver.

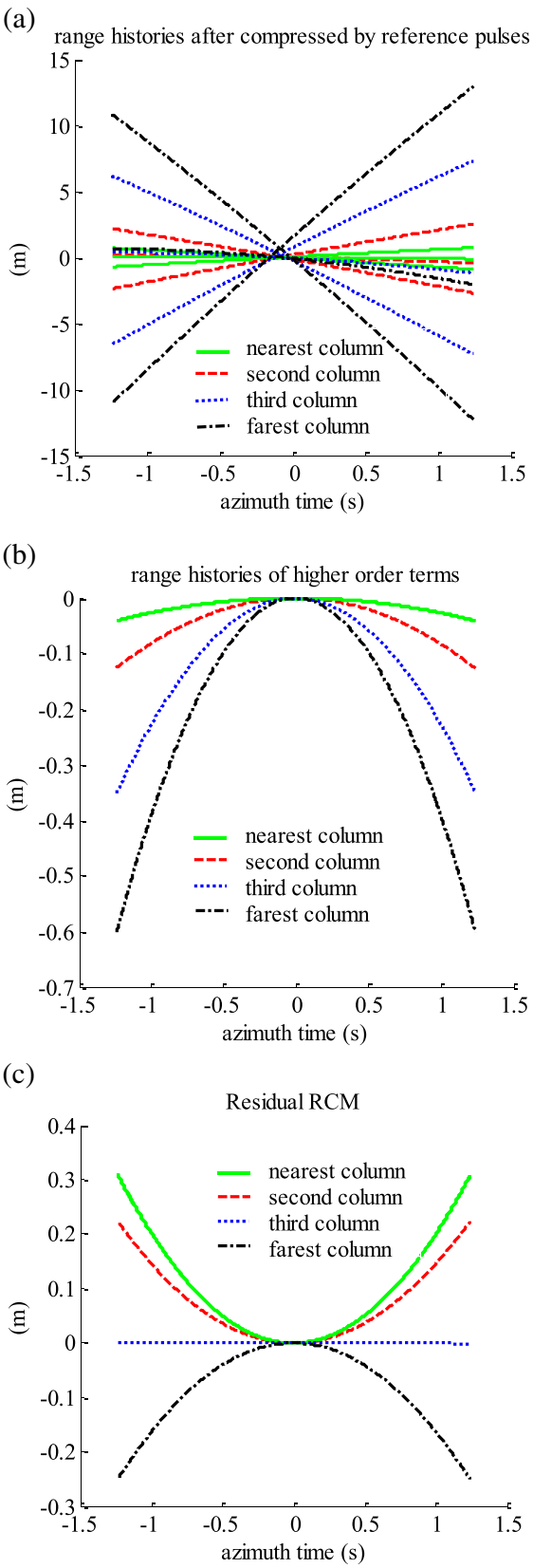

Figure 4 Range history after each processing step.

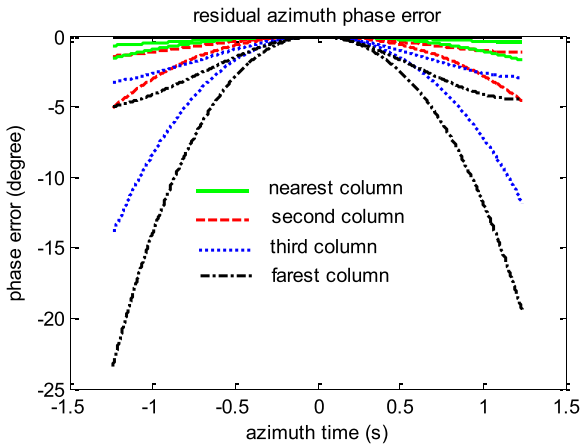

Figure 5 Residual azimuth phase errors.

If the azimuth variation of $\psi_A^h(\xi;\mathbf{r})$ is larger than π/4, an additional step of sub-segment azimuth processing is needed. This means to cut the above image into several small segments along azimuth direction (according to the azimuth variation of $\psi_A^h(\xi;\mathbf{r})$), and then to perform an inverse Fourier transform to get the azimuth time domain signal for each segment. The differential phase between $\psi_A^h(\xi;\mathbf{r})$ of this segment and the phase of $H_{\mathrm{Ac}}(\xi;\mathbf{r})$ for each range gate can be calculated through range history, and be compensated for this segment. Finally, all the segments are transformed to the frequency domain and combined together to get the final fine focused image.

Geocoding

As can be seen from Equation (34), the axes of the focused image are τ and f_ξ, whose limitations are $[\tau_1 : 1/f_s : \tau_1 + (N_r - 1)/f_s]$ and $[-f_{\mathrm{PRF}}/2 : f_{\mathrm{PRF}}/N_a : f_{\mathrm{PRF}}/2]$, respectively. Here, N_r is the image size in range direction and N_a is the size in azimuth direction. f_s is the sample rate and f_{PRF} is the PRF. τ_1 corresponds to the sample delay of the first range gate after range compression. When trigger time of the echo channel is the same as that of the direct pulse channel, then $\tau_1 = R_D(0)/c$.

The position of target $\mathbf{r}$ in the image plane is as follows

$$\begin{cases} \tau_{\mathbf{r}} = \dfrac{R_{bic}(0;\mathbf{r})}{c} \\ f_{\xi_{\mathbf{r}}} = -\dfrac{A(\mathbf{r})}{\lambda} \end{cases} \tag{35}$$

where

$$\begin{aligned} A(\mathbf{r}) &= \left.\frac{dR_{\mathrm{bic}}(\eta;\mathbf{r})}{dt}\right|_{\eta=0} \\ &= \frac{-\mathbf{V_T}(0)\bullet[\mathbf{r}-\mathbf{R_T}(0)]}{|\mathbf{r}-\mathbf{R_T}(0)|} - \frac{-\mathbf{V_T}(0)\bullet[\mathbf{R_R}-\mathbf{R_T}(0)]}{|\mathbf{R_R}-\mathbf{R_T}(0)|} \end{aligned} \tag{36}$$

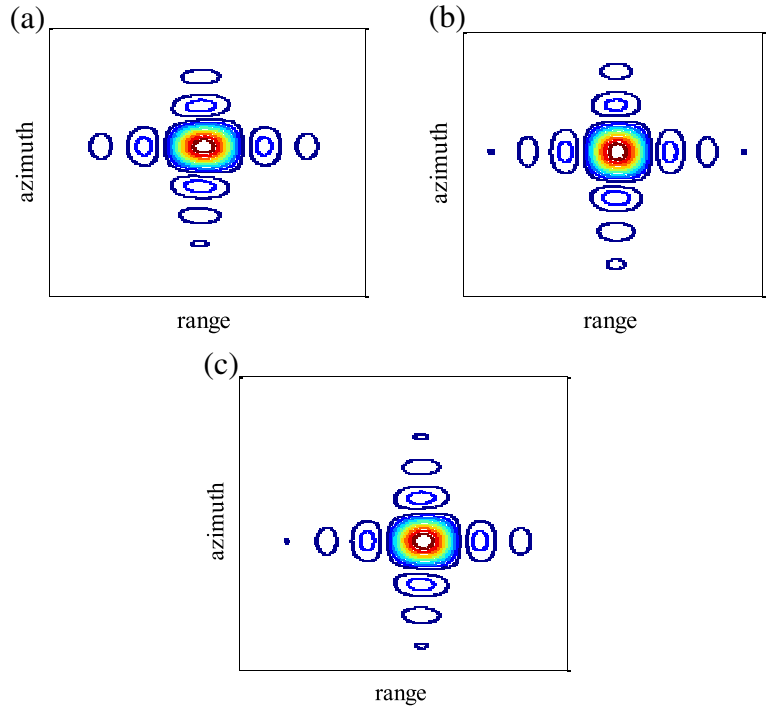

Figure 6 Imaging result of the simulated targets.

Here, $\mathbf{V_T}$ is the transmitter velocity vector in the Earth-fixed coordinates. If a DEM of the scenario is provided, then geocoding can be done according to Equations (1), (2), (10), (35), and (36).

Block diagram of the algorithm

The block diagram of the proposed algorithm for one-stationary bistatic SAR of spotlight-mode is shown in Figure 2. It can be seen that the algorithm is quite efficient as only a pair of range Fourier transforms and a single azimuth Fourier transform are needed for the non-severe azimuth variant case.

Simulation and experimental results

To testify this algorithm, both simulated bistatic SAR data and the real experimental data of HITCHHIKER are processed using this algorithm, and results are analyzed and compared in this section.

Table 2 Interferometry phases of the simulated targets

Target	Differential phase (degree)		Phase error (degree)
	Measured from images	Ideal value	
N	156.9894	157.1157	−0.1263
M	−55.1917	−55.0924	−0.0993
F	76.2087	76.1398	0.0689

Point target simulation

The parameters of point target simulation are according to the TerraSAR-X/HITCHHIKER bistatic experiment in Siegen, Germany. The locations of the stationary receiver and the scene center described by [latitude, longitude, height] are [50.910787 deg, 8.027111 deg, 434.91 m] and [50.913650 deg, 8.059843 deg, 292 m], respectively. The transmitter and receiver parameters are shown in Table 1 and the locations of simulated targets in East-North-Height coordinates with the receiver as the origin are shown in Figure 3. These targets represent the main scenario area of the real experiment. In order to observe the azimuth variation of the range history, each column of targets has the same bistatic range, so each column of targets are on an ellipse arc.

After the range compressing using reference pulses, the residual range histories (without the constant term) of the simulated targets are shown in Figure 4. It can be seen that the RCMs are different for different targets. From Figure 4a, we can see that, for each column of targets, the liner components of their RCMs are changing with their azimuth location. This is consistent with Equation (12). The residual RCMs after the linear terms have been removed by the Keystone Transform are shown in Figure 4b. It can be seen that the residual RCMs are mainly range variant. The targets within the same column (which have the same bistatic range when $\eta = 0$) have almost the same residual RCMs. After the

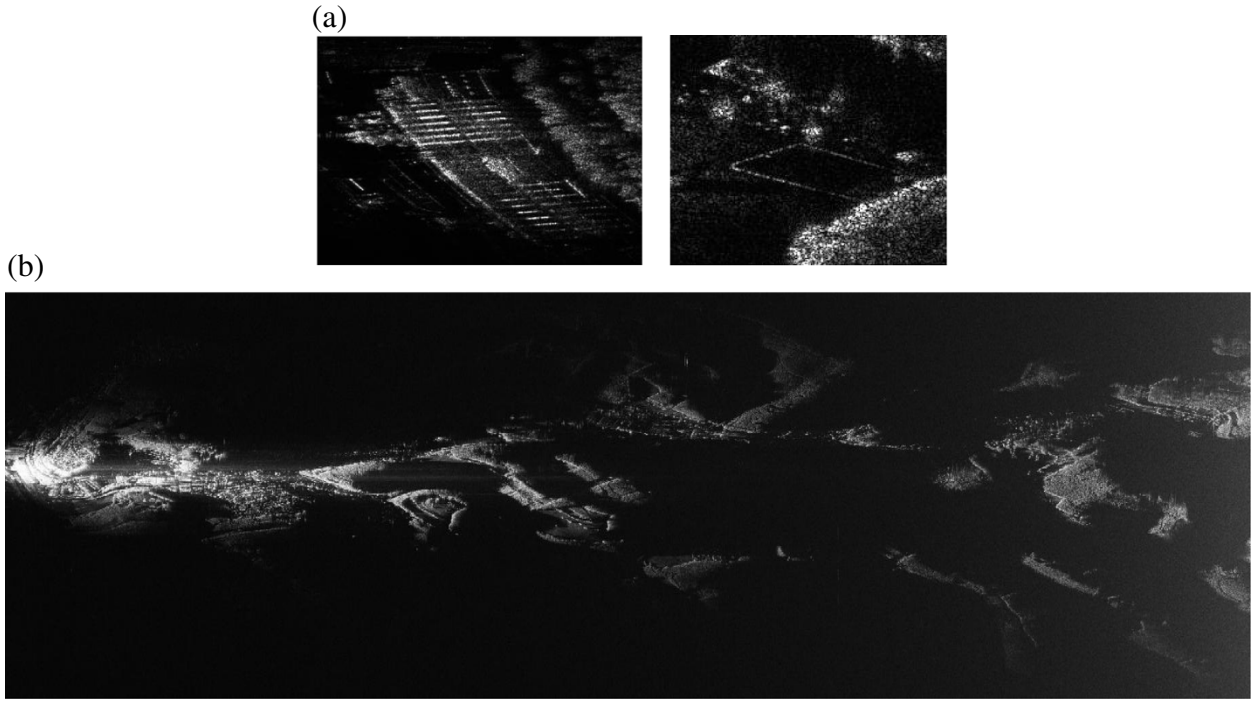

Figure 7 Imaging result of the experimental data processed by the proposed algorithm without geocoding.

bulk residual RCM correction by H_{comp}, the residual RCMs for the simulated targets are all smaller than 0.35 m (see Figure 4c). This is smaller than half a range resolution cell (a range resolution cell is about 0.886 m here), so the range variant residual RCM correction can be omitted in this case. The residual azimuth phases after azimuth phase compensation for each range gate using H_{Ac} are shown in Figure 5. It can be seen that the azimuth phase errors for all the targets in the scene are smaller than 25°, so the subsegment processing step is not needed in this simulation. The imaging results are shown in Figure 6. It can be seen that targets at different locations are all well focused.

To testify the phase preserving ability of this algorithm, and to answer the question: whether the image processed by this algorithm is able to do the further interferometry processing, another set of raw data is simulated. All the parameters are the same with the first raw data, except that the receiver's location described by [latitude, longitude, height] is [50.910787 deg, 8.027111 deg, 435.91 m]. The differential phases of target N, M, F are shown in Table 2, from which we can see that the differential phases are very close to the ideal differential phases calculated by $-\frac{2\pi}{\lambda}\left[R_{\text{bic}}(0;\mathbf{r}) - R_{\text{bic}}^{\text{new}}(0;\mathbf{r})\right]$, where $R_{\text{bic}}^{\text{new}}$ means the range corresponding to the second receiver. The variance of the differential phase errors of all the simulated targets is 0.0919°. This means that the algorithm provided here is well phase preserving and can support the interferometry processing.

Experimental data processing and results

The experimental data of the TerraSAR-X/HITCH-HIKER bistatic SAR experiment is processed by the proposed algorithm. The focused image before geocoding of the scenario is shown in Figure 7b, and zoomed patches of the image are shown in Figure 7a, from which we can see that the image is well focused.

The image is then geocoded based on the DEM data of the scenario. Overlay the image on to Google earth, all the buildings and roads match very well with the orthophoto, which validates the correctness of the geocoding method in "Geocoding" section. The geocoded image by proposed algorithm is compared with the imaging result of BP algorithm in Figure 8. It can be seen that the imaging result of the algorithm provided here can compare beauty with the result of BP algorithm. In the imaging results, the buildings are well focused, while the trees are a little blur because the weather is windy while data acquisition. The same size (4096*6000) image processed by the algorithm here using Matlab on a single PC takes about 5 min, while processed by BP algorithm on the same PC takes more than 31 h, which validates the efficiency of this algorithm.

Conclusion

This article proposed an imaging algorithm for the one-stationary bistatic SAR in spotlight mode. The main

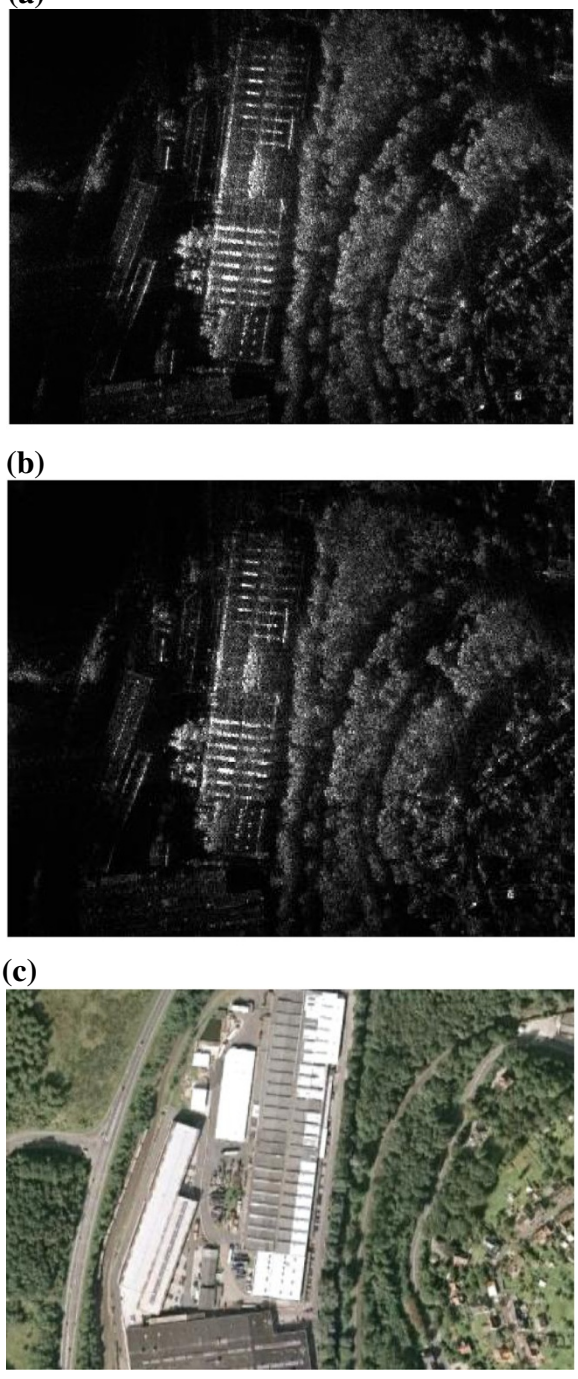

Figure 8 Comparison of the geocoded image results processed by the proposed algorithm and by BP algorithm.

property of the algorithm is using the Keystone Transform to correct the linear part of the two-dimensional variant RCM. The algorithm can directly be applied to the bistatic SAR data which has been range compressed by the reference pulses; therefore, it is efficient and convenient to use. Both simulation and experimental data processing results validate the algorithm.

Competing interests

The authors declare that they have no competing interests.

Authors' information

Xiaolan Qiu (M'09) received the B.S. degree in electronic engineering from the University of Science and Technology of China in 2004 and the Ph.D. degree in signal and information processing from the Graduate University of the Chinese Academy of Sciences, Beijing, China, in 2009. Since 2009, she has been working in the Institute of Electronics, Chinese Academy of Sciences (IECAS). From May to October 2011, she was supported by K.C. Wong Education Foundation Hong Kong and being a guest scientist in the Center for Sensorsystems (ZESS), University of Siegen. Her current research interests include mono- and bistatic SAR signal processing, SAR interferometry and geostationary orbit SAR.

Florian Behner received the Dipl.Ing. degree in electrical engineering from the University of Siegen, Siegen, Germany, in 2009. He is a research assistant at the Center for Sensorsystems, University of Siegen, Siegen, Germany since 2009 and member of the MOSES postgraduate programme. His current research interests include radar sensor development, bistatic SAR processing and noise SAR. Mr. Behner is member of the DPG (German Physical Society).

Simon Reuter received the Dipl.Ing. degree in electrical engineering from the University of Siegen, Siegen, Germany, in 2009. He is a research assistant at the Center for Sensorsystems, University of Siegen, Siegen, Germany since 2009 and member of the MOSES postgraduate programme. His current research interests include radar sensor development, bistatic SAR processing and noise SAR. Mr. Reuter is member of the VDE Association for Electrical, Electronic and Information Technologies.

Holger Nies(M'10) received the Diploma degree in electrical engineering and the Dr. Eng. degree, from the University of Siegen, Siegen, in 1999 and 2006, respectively.

Since 1999 he is a member of the Center for Sensorsystems (ZESS) at the University of Siegen and a lecturer in the Department of Signal Processing and Communication Theory. Since 2010 he is executive director of the International Postgraduate Programme (IPP) "Multi Sensorics" and of the NRW Research School on Multi-Modal Sensor Systems for Environmental Exploration and Safety (MOSES) at the university of Siegen. He is team leader of the SAR group of the ZESS.

He worked in the project sector "Optimal Signal Processing, Remote Sensing - SAR" of ZESS since 1999. He was involved in some project work for Daimler AG (Stuttgart, Germany) in the field of engine modeling and optimization. He was working in the area of SAR interferometry for the German TerraSAR-X mission. Currently he is leading a BMBF funded project regarding optimal processing of TanDEM-X data. His current research interests include bistatic SAR processing, SAR interferometry and distributed data fusion.

Otmar Loffeld(M'05–SM'06) received the Diploma degree in electrical engineering from the Technical University of Aachen, Aachen, Germany, in 1982 and the Eng. Dr. degree and the "Habilitation" in the field of digital signal processing and estimation theory from the University of Siegen, Siegen, Germany, in 1986 and 1989, respectively.

In 1991, he was appointed as a Professor for digital signal processing and estimation theory at the University of Siegen. Since then, he has given lectures on general communication theory, digital signal processing, stochastic models and estimation theory, and synthetic aperture radar. In 1995, he became a Member of the Center for Sensorsystems (ZESS), which is a central scientific research establishment at the University of Siegen (www.zess.uni-siegen.de), where he has been the Chairman since 2005. In 1999, he became the Principal Investigator (PI) on baseline estimation for the X-band part of the Shuttle Radar Topography Mission, where ZESS contributed to the German Aerospace Center's baseline calibration algorithms. He is the PI for the interferometric techniques in the German TerraSAR-X mission, and together with Prof. Ender from FGAN, he is one the PIs for a bistatic spaceborne airborne experiment, where TerraSAR-X serves as the bistatic illuminator while FGAN's PAMIR system mounted on a Transall airplane is used as a bistatic receiver. In 2002, he founded the International Postgraduate Program "Multi Sensorics," and based on that program, he established the "NRW Research School on Multi Modal Sensor Systems for Environmental Exploration and Safety (www.moses-research.de)" at the University of Siegen as an upgrade of excellence, in 2008. He is the Speaker

and the Coordinator of both doctoral degree programs, hosted by ZESS. Furthermore, he is the university's Scientific Coordinator for "Multidimensional and Imaging Systems." He is the author of two textbooks on estimation theory. His current research interests include multisensor data fusion, Kalman filtering techniques for data fusion, optimal filtering and process identification, SAR processing and simulation, SAR interferometry, phase unwrapping, and baseline estimation. A recent field of interest is bistatic SAR processing.

Prof. Loffeld is a member of the Information Technology Society of the Association for Electrical, Electronic and Information Technologies and a senior member of the IEEE/GRSS. He was the recipient of a Scientific Research award from Northrhine-Westphalia ("Bennigsen-Foerder Preis") for his works on applying Kalman filters to phase estimation problems such as Doppler centroid estimation in SAR, and phase and frequency demodulation.

Lijia Huang(M'10) received the B.S. degree in electronic engineering from Beihang University, Beijing, China, in 2006 and the Ph.D. degree in signal processing and information science at the Graduate University of Chinese Academy of Sciences, Beijing, China, in 2011.

Since 2011, she has been working in the Institute of Electronics, Chinese Academy of Sciences (IECAS). Her current research interests include geostationary orbit SAR and SAR interferometry.

Donghui Hu received the B.S. degree from Peking University, Beijing, China, in 1992, and the M.S. degree from the Beijing Institute of Technology, Beijing, in 2001.

He is currently an Associate Research Fellow with the Institute of Electronics, Chinese Academy of Sciences, Beijing.

His main research interests include SAR signal processing, SAR interferometry and SAR calibration.

Chibiao Ding received the B.S. and Ph.D. degrees in electronic engineering from Beihang University, Beijing, China, in 1997.

Since then, he has been working with the Institute of Electronics, Chinese Academy of Sciences, Beijing, where he is currently a Research Fellow and the Vice Director. In 2006, he got the first prize in China's State Technological Invention Award.

His main research interests include advanced SAR systems, signal processing technology, and information systems.

Acknowledgments

This study was supported in partly by the Special Foundation of President of the Chinese Academy of Sciences, the National Science Foundation of China (No. 61101200), and the authors are gratefully acknowledging the support of K.C. Wong Education Foundation Hong Kong.

Author details

[1]Institute of Electronics, Chinese Academy of Sciences, Beijing 100190, China. [2]Key Laboratory of Spatial Information Processing and Applied System, Chinese Academy of Sciences, Beijing 100190, China. [3]Center for Sensorsystems (ZESS), University of Siegen, Siegen 57076, Germany.

Received: 8 March 2012 Accepted: 2 September 2012
Published: 12 October 2012

References

1. O Loffeld, H Nies, V Peters, S Knedlik, Models and useful relations for bistatic SAR processing. IEEE Trans. Geosci. Remote Sens. **42**(10), 2031–2038 (2004)
2. R Wang, O Loffeld, YL Neo, H Nies, Z Dai, Extending Loffeld's bistatic formula for the general bistatic SAR configuration. IET Radar Sonar Navigat **4**(1), 74–84 (2010)
3. JHG Ender, Signal theoretical aspects of bistatic SAR, in *Proceedings of IGARSS'03, vol. 3*, ed. by (Toulouse, France, 2003), pp. 1438–1441
4. Q Xiaolan, H Donghui, D Chibiao, An Omega-K algorithm with phase error compensation for bistatic SAR of a translational invariant case. IEEE Trans. Geosci. Remote Sens. **46**(8), 2224–2232 (2008)
5. R Bamler, F Meyer, W Liebhart, No math: bistatic SAR processing using numerically computed transfer functions, in *IGARSS 2006*, ed. by (Denver, Colorado, 2006), pp. 1844–1847
6. R Bamler, F Meyer, W Liebhart, Processing of bistatic SAR data from quasi-stationary configurations. IEEE Trans. Geosci. Remote Sens. **45**(11), 3350–3358 (2007)
7. D D'Aria, AM Guarnieri, F Rocca, Focusing bistatic synthetic aperture radar using dip move out. IEEE Trans. Geosci. Remote Sens. **42**(7), 1362–1376 (2004)
8. Z Zhenhua, X Mengdao, D Jinshan, B Zheng, Focusing parallel bistatic SAR data using the analytic transfer function in the wavenumber domain. IEEE Trans. Geosc. Remote Sens. **45**(11), 3633–3645 (2007)
9. N Yew Lam, F Wong, IG Cumming, A two-dimensional spectrum for bistatic SAR processing using series reversion. IEEE Geosci. Remote Sens. Lett. **4**(1), 93–96 (2007)
10. F Behner, S Reuter, HITCHHIKER—hybrid bistatic high resolution SAR experiment using a stationary receiver and TerraSAR-X transmitter, in *2010 8th European Conference on Synthetic Aperture Radar (EUSAR)*, ed. by (Aachen, Germany, 2010), pp. 1–4
11. JHG Ender, J Klare, I Walterscheid, M Weiss, C Kirchner, H Wilden, O Loffeld, A Kolb, W Wiechert, M Kalkuhl, S Knedlik, U Gebhardt, H Nies, K Natroshvili, S Ige, AM Ortiz, A Amankwah, *Bistatic exploration using spaceborne and airborne SAR sensors: a close collaboration between FGAN, ZESS, and FOMAAS* (IGARSS 2006, Denver, Colorado, 2006), pp. 1828–1831
12. P Dubois-Fernandez, H Cantalloube, B Vaizan, G Krieger, R Horn, M Wendler, V Giroux, ONERA-DLR bistatic SAR campaign: planning, data acquisition, and first analysis of bistatic scattering behaviour of natural and urban targets. IEE Proc. Radar Sonar Navigat. **153**(3), 214–223 (2006)
13. I Walterscheid, T Espeter, AR Brenner, J Klare, JHG Ender, H Nies, R Wang, O Loffeld, Bistatic SAR experiments with PAMIR and TerraSAR-X—setup, processing, and image results. IEEE Trans. Geosci. Remote Sens. **48**(8), 3268–3279 (2010)
14. T Espeter, I Walterscheid, J Klare, AR Brenner, JHG Ender, Bistatic forward-looking SAR experiments using an airborne receiver, in *International Radar Symposium (IRS)*, ed. by (Germany, 2011), pp. 41–46
15. J Sanz-Marcos, P Lopez-Dekker, JJ Mallorqui, A Aguasca, P Prats, SABRINA: a SAR bistatic receiver for interferometric applications. IEEE Trans. Geosci. RemoteSens. Lett. **4**(2), 307–311 (2007)
16. Z Zeng, M Antoniou, F Liu, *First space surface bistatic fixed receiver SAR images with a navigation satellite* (International Radar Symposium (IRS), Germany, 2011), pp. 373–378
17. X Qiu, D Hu, C Ding, Non-linear chirp scaling algorithm for one-stationary bistatic SAR, in *Synthetic Aperture Radar (APSAR) 2007*, ed. by (Shanghai, China, 2007), pp. 111–114
18. Q Xiaolan, H Donghui, D Chibiao, An improved NLCS algorithm with capability analysis for one-stationary BiSAR. IEEE Trans. Geosci. Remote Sens. **46**(10), 3179–3186 (2008)

doi:10.1186/1687-6180-2012-221
Cite this article as: Qiu *et al.*: An imaging algorithm based on keystone transform for one-stationary bistatic SAR of spotlight mode. *EURASIP Journal on Advances in Signal Processing* 2012 **2012**:221.